Stress-assisted nucleation and growth of γ″ and γ′ precipitates in a Cu-1.2wt%Be-0.1wt%Co alloy aged at 320°C

Stress-assisted nucleation and growth of γ" and γ' precipitates in a Cu-1.2wt%Be-0.1wt%Co alloy aged at 320°C

Journal:	*Philosophical Magazine & Philosophical Magazine Letters*
Manuscript ID:	TPHM-11-Sep-0359.R1
Journal Selection:	Philosophical Magazine
Date Submitted by the Author:	20-Dec-2011
Complete List of Authors:	MONZEN, Ryoichi; Kanazawa University, Innovative Technology and Science OKAWARA, Syoichi; Kanazawa University, Division of Mechanical Science and Engineering WATANABE, Chihiro; Kanazawa University, Division of Innovative Technology and Science
Keywords:	copper alloys, precipitation, nucleation, growth, stresses, growth processes
Keywords (user supplied):	

Stress-assisted nucleation and growth of γ" and γ' precipitates in a Cu-1.2wt%Be-0.1wt%Co alloy aged at 320°C

Ryoichi Monzen[a], Syoichi Okawara[b] and Chihiro Watanabe[c]

[a]Corresponding author, *Division of Innovative Technology and Science, Kanazawa University, Kakuma-machi, Kanazawa 920-1192, Japan,* TEL: +81-76-234-4678, FAX: +81-76-264-6495, Email: monzen@t.kanazawa-u.ac.jp

[b]*Division of Mechanical Science and Engineering, Kanazawa University, Kakuma-machi, Kanazawa 920-1192, Japan,* TEL: +81-76-234-4678, FAX: +81-76-264-6495, Email: ogawara@metal.ms.t.kanazawa-u.ac.jp

[c]*Division of Innovative Technology and Science, Kanazawa University, Kakuma-machi, Kanazawa 920-1192, Japan,* TEL: +81-76-234-4677, FAX: +81-76-264-6495, Email: chihiro@t.kanazawa-u.ac.jp

Stress-assisted nucleation and growth of γ" and γ' precipitates in a Cu-1.2wt%Be-0.1wt%Co alloy aged at 320°C

An investigation by high-resolution transmission electron microscopy of the precipitation process during ageing a Cu-1.2wt%Be-0.1wt%Co alloy at 320°C has revealed that the transition phases follow a γ"→ γ" + γ' → γ sequence. The γ' phase heterogeneously precipitates on the γ" phase. The effects of an external stress on the nucleation and growth of disc-shaped γ" and plate-shaped γ' precipitates have been examined for the alloy aged at 320°C. A compressive stress applied in the [001] direction during ageing preferentially accelerates the nucleation and growth of the γ" variant normal to the [001] axis amongst crystallographically-equivalent three ones and the specific four γ' variants formed on the γ" variant normal to the [001] axis. A tensile stress does not significantly affect those of γ" and γ' precipitates. The critical diameter of the disc-shaped γ" nucleus is estimated as about 1 nm from evaluation of the interaction energy between the applied stress and the misfit strains of γ" precipitates. It is proposed that applied external stress does not affect the diffusion rate but the interphase boundary velocity.

Key words: Cu-Be alloy; γ" and γ'precipitates; nucleation and growth; applied stress; growth kinetics; misfit; interaction energy

1. Introduction

It is widely known that application of an elastic stress during the ageing process of many age-hardenable alloy systems significantly affects the resulting microstructures, in particular the distribution of strengthening precipitates [1-10]. Particularly, for Al-Cu alloys, the effect of directional stress on the orientation distribution of precipitate structures has been invetigated extensively [2, 5, 7, 9]. For example, Eto et al. [5] observed that application of the external stress during ageing below 180°C induced the oriented precipitation of disc-shaped Guinier-Preston (GP) zones and plate-shaped θ' phase in an Al-3.71Cu alloy (All compositions in this text are in weight per cent). Tensile stress along the [001] axis produced the preferential formation of (100) and (010) variants of GP zones and θ', and compressive stress (001) variants. Using a two-step ageing (ageing at 80°C under stress and ageing at 170°C under no stress) procedure, they showed that the stress-orienting effect was initiated and determined during the nucleation stage, namely the formation of GP [I], which will grow to θ' via GP[II]. Recently, Zhu and Starke [9] determined the dependence of orienting of θ'' (GP[II]) and θ' precipitates on the applied stress, ageing temperature and the copper content, using single crystals of Al-2.5Cu and Al-4Cu alloys and a cube-textured Al-5Cu alloy aged to peak strength under compressive stresses. The effect was discussed and explained within the frame of classical nucleation and growth theories that incorporate the interaction energy between the external stress and the lattice misfits of θ'' and θ' precipitates. However, no direct evidence has been provided for the effect of external stress on each of the nucleation and growth of each variant of GP zones or θ'' or θ' precipitates, as yet.

In a previous letter [10], Monzen et al. have shown by transmission electron microscopy (TEM) that application of the external stress during ageing at 200°C

induces the oriented precipitation of disc-shaped GP zones in single crystals of a Cu-0.9Be alloy. Compressive stress along the $[001]_\alpha$ direction assists preferential formation of the GP zones perpendicular to the stress axis and tensile stress induces the same parallel to the stress axis. It has also been revealed that the effect of applied stress is on the nucleation process of GP zones. In addition, the misfit strains $\varepsilon_{11}=\varepsilon_{22}$ and ε_{33} of the GP zone in directions parallel and perpendicular to the plate plane have been estimated from measurements of the length change and lattice parameter during ageing. Very recently, Monzen et al. [11] have found that application of compressive stress in the [001] direction during ageing a Cu-1.2Be-0.1Co alloy at 220°C promotes particularly the nucleation and growth of disc-shaped GP zones normal to the [001] axis. Moreover, investigations by high-resolution (HR) TEM [12] of the precipitation processes in the Cu-0.9Be single crystals containing only the GP zones on the $(001)_\alpha$ plane have revealed that the transition phases follow a more complicated GP zone → γ" → γ'_I → γ_I + γ' → γ sequence than that previously reported, GP zone → γ" → γ' → γ [13]. The disc-shaped GP zones consist of monolayers of Be atoms on the $\{100\}_\alpha$ planes and transform continuously to the γ_I phase via γ" and γ'_I [12]. These metastable phases are composed of alternative Be and Cu matrix layers parallel to the $\{100\}_\alpha$ planes, and have crystallographically-equivalent three variants each. As soon as the structure of γ'_I changes into that of γ_I, the metastable γ' phase heterogeneously precipitates on the γ_I phase and rapidly grows. The γ' phase has twelve variants. The final γ' → γ phase transformation also takes place successively. Moreover, Watanabe et al. [14] have determined the misfit strains of γ", γ'_I, γ' and γ precipitates from measurements of the length change and the lattice parameter on ageing using the Cu-0.9Be single crystals containing only the GP zones on the $(001)_\alpha$ plane. Table 1 lists the estimated misfit

strains of the GP zone [10] and the γ", γ' and γ phases.

Since the disc-shaped γ" phase has almost the same misfit strains as the disc-shaped GP zone as seen in Table 1, if a solutionized Cu-Be specimen is aged under an applied compressive or tensile stress at a temperature at which the γ" phase is directly formed, the same stress-oriented formation of γ" as that of the GP zones is expected. In fact, we have found the stress-oriented nucleation of the γ" precipitates, which depends on the sense of the applied stress, and furthermore observed the heterogeneous formation of γ' on the γ" phase, as will be shown later. In this work, the effects of an applied compressive or tensile stress on the nucleation and growth of each variant of the γ" and γ' phases are examined for a Cu-1.2Be-0.1Co alloy aged at 320°C. The critical diameter of the disc-shaped γ" precipitation nucleus is also determined. In addition, the growth kinetics of precipitates under external stress is discussed.

2. Experimental

Cu-1.2Be-0.1Co alloy ingots were prepared from 99.99Cu and Cu-3.81Be and Cu-10.45Co master alloys by melting in a vacuum. The addition of 0.1Co aims to suppress discontinuous precipitation reactions [15]. The alloy ingots were homogenized at 900°C for 48 h in a vacuum, cold-rolled to a 50% reduction in thickness and then spark-cut into specimen strips. For compressive ageing, the specimens had a cross-section of 3 mm × 6 mm and a length of 10 mm. For tensile ageing, the specimens had the same cross-section but a gauge length of 20mm. All the specimens were solution-treated at 820°C for 2h in a vacuum and quenched into water. The solution treatment also caused complete recrystallization of the specimens. The solution-treated specimens were then aged at 320°C for various times either under an applied stress of 70MPa (stress ageing) or under no stress (free ageing). The applied stress of 70MPa was about half of the yield

strength of the solution-treated specimen at 320°C. The temperature of 320°C was chosen because ageing a Cu-1.2Be alloy at a temperature between about 270 and 350°C causes the direct nucleation of γ" precipitates, according to the solvus lines for the GP zones and γ" previously reported [16]. Also an X-ray analysis was performed to measure the lattice parameters of the solution-treated and aged specimens. A diffractmeter with a Cu target was used for the X-ray analysis.

Thin foils, 0.2 mm thick, for TEM observations were prepared by grinding the aged specimens with SiC papers and by electropolishing using a solution of 67% methanol and 33% nitric acid at −30°C and 6.5 V in a twin-jet electropolisher. Microscopy was performed using a HITACHI H-9000NAR and a JEOL 2010FEF microscope operated at 300 and 200 kV, respectively. HRTEM images were taken with the objective lens at or near to Scherzer defocus. Small variations in the defocus did not significantly affect the appearance of lattice fringes of precipitates. All HRTEM images were obtained with the beam parallel to a $<110>_{\alpha}$ direction in the Cu matrix. This is the optimum foil orientation for identifying each of the γ", γ'_{I}, γ_{I}, γ' and γ phases [12, 14]. Lattice fringe spacings in precipitates were measured on enlarged HRTEM images, using the Cu matrix $\{111\}_{\alpha}$ fringes as a standard.

3. Results

3.1. *Applied stress effect on age hardening curve*

Figure 1 shows the ageing time dependence of the Vickers hardness of the Cu-1.2Be-0.1Co specimens, free-aged (FA), tensile-stress-aged (TSA) and compressive-stress-aged (CSA) at 320°C up to 9h. The microhardness of the CSA specimen initially increases more rapidly than that of the FA specimen and, after ageing for 9h, the

hardness of both specimens becomes almost the same value. On the other hand, application of the tensile stress of 70MPa does not significantly change the hardness throughout the ageing process. As will be noticed later, the higher hardness at each time up to 8h for the CSA specimen is mainly caused by the promotion of nucleation of γ" precipitates and heterogeneous nucleation of γ' phase on γ" under compressive stress.

3. 2. *Nucleation of γ" phase and precipitation process*

Figure 2 depicts a HRTEM image of precipitates in the Cu-Be-Co specimen, FA at 320°C for 2 h. The zone axis is parallel to $[110]_\alpha$ of the Cu matrix. The precipitates have a two Be-layer structure separated by a matrix layer parallel to $(001)_\alpha$. Lattice fringes parallel to $(1\bar{1}0)_\alpha$ also are visible. The spacings of the lattice fringes parallel to the $(001)_\alpha$ ($//(001)_{\gamma"}$) and $(1\bar{1}0)_\alpha$ ($//(0\bar{1}0)_{\gamma"}$) planes are measured as c=0.29nm and b=0.25nm, respectively. The angle α between the $(001)_{\gamma"}$ and $(0\bar{1}0)_{\gamma"}$ planes is obtained as α=90°. These values are in agreement with a=b=0.254nm and c=0.292nm and α=β=γ=90° for the γ" phase [12]. The disc-shaped γ" precipitates on the left and right sides of Figure 2 have diameters of about 5 and 3nm, which is the smallest of observed γ" precipitates. Monzen et al. [10, 12] have shown that, in a Cu-0.9Be alloy aged at 200°C, disc-shaped GP zones are first nucleated and transform continuously to the γ" phase over about 10nm in diameter, which has a two Be-layer structure separated by a matrix layer parallel to $\{001\}_\alpha$. Therefore we conclude that the γ" phase does not consecutively transform from the GP zone but is directly nucleated during ageing the present Cu-Be-Co alloy at 320°C.

Monzen et al. [12] and Watanabe et al. [14] have reported from HRTEM observations that the transition phases in Cu-0.9Be alloy single-crystals aged at 200 to

420°C [12] and Cu-1.8Be-0.2Co alloy polycrystals aged at 320°C [14] follow a GP zone → γ" → γ'_I → γ_I+γ' → γ sequence with ageing time. The disc-shaped GP zones transform continuously to the γ_I phase via γ" and γ'_I. These metastable phases are composed of alternative Be and Cu matrix layers parallel to $\{100\}_\alpha$. The γ' phase heterogeneously precipitates on the γ_I phase having about ten Be-layers and transforms successively to the equilibrium γ phase. In this work, however, the structure of γ" was maintained up to six Be-layers and then the heterogeneous formation of γ' occurred on the γ" phase which consisted of six Be-layers, as exemplified in Figure 3. Prolonged ageing for 240 h generated the successive transformation from γ' to γ. Thus, the transition phases in this study follow a γ"→ γ"+γ' → γ sequence with ageing time.

Figure 4a depicts a HRTEM image of a precipitate composed of the γ" and γ' phases in the specimen aged at 320°C for 6 h. Figure 4b is an enlarged image of the outlined frame in Figure 4a after noise filtering by fast Fourier transformation and inverse fast Fourier transformation. As schematically illustrated in Figure 4c, a misfit dislocation with a Burgers vector $\boldsymbol{b} = [001]_{\gamma"}$ is observed at the interface between the γ" phase and the Cu matrix. Five $(001)_{\gamma"}$ spacings on the γ" phase side of the interface are matched with four $(001)_\alpha$ spacings on the Cu side of the interface. The fact that the heterogeneous precipitation of γ' occurs on the γ" phase consisting of six Be-layers strongly suggests that the misfit dislocation at the interface between the γ" phase and the Cu matrix promotes the heterogeneous formation of γ'.

3. 3. *Effect of external stress on nucleation and growth of γ" phase*

Figures 5a, 5b and 5c are examples of TEM images and corresponding selected-area diffraction patterns (SADP) of the specimens, FA, CSA and TSA at 320°C for 3 h. The

TEM images were taken using an incident beam parallel to the $[100]_\alpha$ direction. In Figure 5a, intensity maxima in the streaks along the $<002>_\alpha$ directions in the SADP are seen near the $2/3\{002\}_\alpha$ reciprocal-lattice positions. This is a feature of γ" precipitates [12, 13] and indicates the formation of γ" precipitates parallel to the (010) and (001) planes. Although no γ" precipitates parallel to (100) are observed in Figure 5a, the γ" precipitates are, of course, equally present in the FA specimen. Contrary to the FA specimen, the stress-aged specimens showed preferential formation of γ" precipitates parallel to particular {100} planes, depending on the sense of the applied stress. That is, compressive or tensile stress along [001] produces preferentially γ" precipitates perpendicular to or parallel to the stress axis (Figures 5b and 5c), as might be expected.

Figure 6 shows the number density of disc-shaped γ" precipitates as a function of stress ageing time *t* for the specimens, CSA and TSA at 320°C for various times *t* and then FA at 320 °C for times *t*', the sum of *t* and *t*' being 3 h. The number density of γ" precipitates is defined as the volume fraction of γ" precipitates divided by the average volume per one γ" precipitate. The volume fraction was determined by applying the lattice constants of the CSA, TSA and FA specimens measured by an X-ray analysis to the experimental data on the dependence of the lattice constant on the Be concentration in the literature [17]. It is seen in Figure 6 that the density of γ" precipitates in the CSA specimen increases and then becomes constant after about 1.5 h. This observation shows that the formation of the γ" precipitates favored by the compressive stress is completed after 1.5 h. On the other hand, the TSA specimen reveals no significant change in the number density with *t*. No difference in the number density was found between the specimens aged at 2 and 4 h under tensile stress or under no stress, indicating that

ageing for 2 h under tensile stress or no stress is long enough to cause the nucleation of γ" precipitates to be finished.

As revealed in Figure 2 and previously reported [12], the Bain orientation relationship is satisfied between the γ" phase and the surrounding Cu matrix: $(001)_\alpha$ // $(001)_{\gamma"}$; $[110]_\alpha$ // $[100]_{\gamma"}$ (or $[1\bar{1}0]_\alpha$ // $[0\bar{1}0]_{\gamma"}$). This orientation relationship has three variants, as shown in Table 2. The disc-shaped variants I, II and III are parallel to $(001)_\alpha$, $(100)_\alpha$ and $(010)_\alpha$ of the Cu matrix, respectively. We selected the grains in which the stress axis was nearly perpendicular to $(001)_\alpha$ or parallel to $(100)_\alpha$ and $(010)_\alpha$, and determined the number density of each γ" variant from TEM observations using the electron beam parallel to $[110]_\alpha$ or $[011]_\alpha$ and $[101]_\alpha$ of the grains. In this case, the thickness of TEM foils was measured by utilizing the $\{111\}_\alpha$ coherent twin boundary, parallel to $[110]_\alpha$, $[011]_\alpha$ and $[101]_\alpha$. Table 3 summarises the number density of γ" variants I, II and III in the specimens, FA, CSA and TSA for 3 h. The density of the disc-shaped variant I perpendicular to the $[001]_\alpha$ stress axis in the CSA specimen is higer than those of the variants II and III parallel to the stress axis in the CSA specimen and the variants I, II and III in the FA and TSA specimens. The densities of the latter variants are nearly identical except for that of the variant I in the TSA specimen, which is lower.

Figure 7 depicts a TEM image of γ" precipitates in the specimen, aged at 320°C for 2h and then CSA for 1h. The image was taken using the electron beam parallel to $[100]_\alpha$. The diameter of disc-shaped γ" precipitates perpendicular to the $[001]_\alpha$ stress axis is larger than that of γ" precipitates parallel to $(010)_\alpha$. Table 4 lists the diameter of variants I, II and III parallel to $\{001\}_\alpha$ in the specimens, aged at 320°C for 2h and then FA, CSA and TSA for 1h. The stress axis is along $[001]_\alpha$. The diameter of the variant I

parallel to $(001)_\alpha$ in the CSA specimen is larger than those of the variants II and III parallel to the stress axis in the CSA specimen and the variants I, II and III in the FA and TSA specimens. The diameters of the latter variants are almost the same. The average thicknesses of the latter variants estimated from TEM images also were nearly identical, 0.31nm, which is smaller than the thickness of 0.38nm for the variant I in the CSA specimen.

3. 4. *Effect of external stress on nucleation and growth of γ' phase on γ"*

Ageing at 320 °C for 4h under no stress produced γ" precipitates consisting mainly of three Be-layers, whereas in the specimen aged for 3 h and then CSA for 1h, the γ' phase was heterogeneously formed on the γ" phase consisting of three Be-layers, as exemplified in Figure 8. This indicates that the heterogeneous nucleation of γ' on γ" is assisted by compressive stress. On the other hand, ageing for 3 or 4 h under no stress and then for 1 h under tension generated the γ" phase composed primarily of three or five Be-layers but no γ' phase on γ". The specimen FA for 5 h and then TSA for 1 h exhibited the occurrence of the γ' phase on the γ" phase consisting of six Be-layers. It should be recalled that in the FA specimen the heterogeneous formation of γ' occurs on the γ" phase composed of six Be-layers (Figure 3).

An analysis of the SADPs of regions containing γ' precipitates revealed that the γ' precipitates aligned with the Cu matrix according to the following orientation relationships: $(1\bar{1}3)_\alpha$ // $(0\bar{1}3)_\gamma$; $[110]_\alpha$ // $[100]_\gamma$ and $(1\bar{1}\bar{2})_\alpha$ // $(0\bar{1}\bar{2})_\gamma$; $[110]_\alpha$ // $[100]_\gamma$. The orientation relationships are coincident with those reported by Monzen *et al*. [12]. The γ' precipitates had a plate-like shape parallel to $\{113\}_\alpha$ or $\{112\}_\alpha$ (Figure 9) [12, 18]. Each orientation relationship has six variants and thus there are twelve variants in

total, as shown in Table 2. For example, the γ' variants I-1–4 are equally formed on the γ'' variant I parallel to $(001)_\alpha$.

We chose the grains in which the stress axis was nearly perpendicular to $(001)_\alpha$ or parallel to $(100)_\alpha$ and $(010)_\alpha$, and determined the orientations of the γ' precipitates heterogeneously formed on the γ'' precipitates parallel to $\{001\}_\alpha$ using the electron beam parallel to $<110>_\alpha$ of the grains. For example, the orientations of the plate-shaped γ' precipitates parallel to $(1\,\bar{1}\,\bar{2})_\alpha$ and $(1\,\bar{1}\,3)_\alpha$ in Figure 9, taken along $[110]_\alpha$, are identified as I-1 and I-2 from an analysis of the SADP. Table 5 summarises the fraction of the number $N_{3\gamma''+\gamma'}$ of γ'' precipitates composed of three Be-layers with γ' phase to the total number $N_{3\gamma''}$ of γ'' precipitates composed of three Be-layers for the specimen, aged at 320°C for 3h and then CSA for 1h, and that of the number $N_{6\gamma''+\gamma'}$ of γ'' precipitates composed of six Be-layers with γ' phase to the total number $N_{6\gamma''}$ of γ'' precipitates composed of six Be-layers for the specimen, aged at 320°C for 5h and then FA or TSA for 1h. The value of $N_{3\gamma''+\gamma'}/N_{3\gamma''}$ for the variants I-1–4 are much larger than that for the variants II-1–4 and III-1–4, indicating that the formation of the variants I-1–4 is more accelerated by compressive stress. Also there are no essential differences amongst the values of $N_{6\gamma''+\gamma'}/N_{6\gamma''}$ for all the variants in the FA and TSA specimens. Thus ageing under tension does not significantly influence the nucleation of each γ' variant.

By assuming that the shape of the γ' precipitates is a spheroid described in the *x*-*y*-*z* coordinates by $x^2/l^2+y^2/m^2+z^2/n^2\leq 1$, Monzen et al. [12] obtained $l : m : n = 7 : 28 : 59$ in the directions $[1\bar{1}3]_\alpha$, $[110]_\alpha$ and $[\bar{3}32]_\alpha$ for the variant I-2 and the directions $[1\bar{1}\bar{2}]_\alpha$, $[110]_\alpha$ and $[\bar{1}\,11]_\alpha$ for the variant I-1. Table 6 lists the length *n* of plate-shaped γ' variants in the specimens, aged 320°C for 3h, compressive-stress-aged at 320°C for 1h

and then FA, CSA or TSA at 320°C for 2h. The compressive-stress ageing for 1 h after ageing for 3h aimed to cause the formation of the γ' phase on the γ" phase composed of three Be-layers. It is seen in Table 6 that the length of the variants I-1–4 in the CSA specimen is large compared with those of the other variants in the CSA specimen and all the variants in the FA and TSA specimens, which are almost the same. The thicnesses, namely the values of l of the latter variants also were nearly identical, 3.0nm, which is smaller than 3.5nm for the variants I-1–4 in the CSA specimen.

4. Discussion

4. 1. *Effect of interaction energy*

The origin of the promotion of nucleation and growth of the γ" variant I only perpendicular to the stress axis and the four γ' variants I-1–4 formed on the γ' variant I under compression can be understood to arise from the interaction energy due to the presence of negative misfit strain ε_{ij} (stress-free transformation strain) between a γ" or γ' precipitate and an external stress σ_{ij}. The interaction energy F_I is expressed as [19]

$$F_I = -V\sigma_{ij}\varepsilon_{ij}, \qquad (1)$$

where V is the volume of the γ" or γ' precipitate. Since ε_{ij} of the γ" variant I or γ' variants I-1–4 has components of ε_{33}=–0.11 or –0.09 and ε_{11}=ε_{22}=–0.01 or –0.03 (Table 1), equation (1) predicts that compressive stress along the $[001]_\alpha$ direction during ageing particularly accelerates nucleation and growth of the γ" variant I or γ' variants I-1–4. This is in agreement with the results shown in Tables 3, 4, 5 and 6. In addition, the prediction of equation (1) that tensile stress along the [001] direction particularly suppresses formation of the γ" variant I normal to the stress axis is coincident with the

result shown in Table 3.

4. 2. *Critical size of γ" precipitation nucleus*

The number density of γ" precipitates parallel to $(001)_\alpha$ in the specimen, CSA for 3h was determined from TEM observations using the electron beam normal to $(110)_\alpha$. The thickness of TEM foils was measured by utilizing the $(1\bar{1}1)_\alpha$ or $(\bar{1}11)_\alpha$ coherent twin boundary. The number density was plotted as a function of the angle θ between the stress axis and the plane normal of the γ" precipitates. It decreased with increasing θ.

The energy change due to the nucleation of γ" precipitates under a stress is given by equation (1). According to a classical nucleation theory [20], the interaction energy F_I affects the nucleation rate R as written by

$$R \propto \exp\left(-\frac{\left(G^* + F_I^*\right)}{kT}\right) \tag{2}$$

where G^* is the activation energy for nucleation in absence of a stress, F_I^* is the interaction energy associated with nucleation of the γ" precipitate of a critical nucleus volume of V^*, k is Boltzmann's constant and T is the absolute temperature. When the nucleation rate at θ=90° and the applied stress are referred to as R_0 and σ_A, respectively, the nucleation rate normalized is written as

$$\ln\left(\frac{R}{R_0}\right) = -\frac{0.1\sigma_A V^*}{kT}\cos^2\theta \tag{3}$$

using the misfit strains of the γ" phase parallel to $(001)_\alpha$, ε_{33}=–0.11 and ε_{11}=ε_{22}=–0.01 (Table 1). The logarithm of the number density of γ" precipitates normalized by that at θ=90°, corresponding to the relative nucleation rate, is plotted against $\cos^2\theta$ in Figure

10. All the data points fall on a single straight line. The slope of the straight line gives $-0.1\sigma_A V^*/kT=0.34$, according to equation (3). Using $k=1.38\times10^{-23}$ JK^{-1}, $\sigma_A=-70$MPa and $T=593$ K, the activation volume for a critical nucleus is estimated to be $V^*=3.9\times10^{-28}$ m^{-3}. When the critical nucleus of the disc-shaped γ" precipitate are assumed to have a thickness of 0.31nm measured by TEM, the estimate of the nucleus diameter is about 1.1 nm. This value is nearly identical to the nucleus diameter of about 1.0 nm obtained by Eto et al. [21] for the GP[I] zones in Al-Cu alloys.

4. 3. *Growth kinetics*

Precipitation from supersaturated solid solutions is a familiar example of growth in which there is a composition difference across a moving interface. In this case, the motion of the interface requires long-range transport of atoms of various species towards or away from the growing regions. Two extreme cases can be distinguished in principle. In one of these an interphase boundary can move very slowly, even under the influence of high driving forces. The rate of motion will be largely independent of the diffusion rate, and the growth is interface-controlled. The other extreme case is where the boundary is highly mobile compared with the rate of diffusion, so that it will move as rapidly as the required segregation can be accomplished. The growth rate is then determined almost entirely by the diffusion conditions, and is said to be diffusion-controlled [22].

In the interface-controlled growth of a precipitate, the interface velocity v_I is written as [22]

$$v_I = \delta\nu(-\Delta G_m / kT)\exp(-\Delta G_d / kT), \qquad (4)$$

where δ is the interface width, ν is the vibrational attempt frequency, ΔG_m is the free

energy change per atom and ΔG_d is the activation energy for interface transport. The interface velocity for various massive reactions has been found to obey the interface-controlled growth equation [23]. It can be considered that the interface velocity under an external stress σ_{ij} is expressed as

$$v_I = \delta\nu[-(\Delta G_m - \sigma_{ij}\varepsilon_{ij}/V_m)/kT]\exp(-\Delta G_d/kT), \quad (5)$$

where V_m is the molar volume of the precipitate. On the other hand, in the diffusion-controlled growth, theoretically the thickness s of plate-shaped precipitates or the size of spherical precipitates follows a parabolic growth law:

$$s = \alpha\sqrt{t}, \quad (6)$$

where α is the parabolic rate constant and t is the growth time. The length of the plate-shaped precipitate is proportional to the growth time [23]. The thickening of plate-shaped precipitates or grain-boundary allotriomorphs in several alloy systems, for example, Cr-rich precipitates with a lath morphology in a Ni-Cr alloy [24] and plate-shaped γ precipitates in a Cu-Ni-Be alloy [25] has been reported to occur with parabolic growth kinetics, equation (6).

As seen in equations (4), (5) and (6), in a diffusion-controlled reaction a linear dimension of the growing product region is proportional to the square root of the growth time, whereas in an interface-controlled reaction, it is linearly proportional to the time. Thus an interface-controlled boundary of a very small product region may become diffusion-controlled as the region grows larger [22]. Although it has been reported that the thickening and lengthening of plate-shaped precipitates of large sizes in several alloy systems is diffusion-controlled [23], it seems that direct evidence has not been provided for the interface-controlled growth of precipitates as yet. In the present alloy

also, it may be expected that the thickening and lengthening of disc-shaped γ" and plate-shaped γ' precipitates are diffusion-controlled. Unfortunately, we could not examine the dependences of the thickness and length of γ" precipitates on the ageing time, because the heterogeneous nucleation of the γ' phase on the γ" phase occurred during ageing at 320°C for a short time under external stress or no stress after completion of the nucleation of γ". Also, collisions between the γ' precipitates during ageing at 320°C for a short time under external stress or no stress following completion of the heterogeneous nucleation of γ' did not enable us to investigate the ageing time dependence of the thickness and length of γ' precipitates.

Finally we will provide evidence for our idea that external stress does not affect the diffusion rate but the interface velocity (equation (5)), from an examination of the growth of ω phase in a Ti-20Mo alloy aged at 350°C under an applied tensile stress. Previous to this work, Nishizawa et al. [8] investigated the effect of an applied stress on the nucleation of ω phase in the Ti-20Mo alloy aged at 350°C, and showed that a tensile stress applied during ageing promotes the nucleation of ω phase. We have found that application of a tensile stress of 400MPa during ageing the same alloy at 350°C accelerates not only the nucleation but also the growth of ω phase. Figure 11 displays the average diameter of ω precipitates against ageing time t up to 168h (6.048×10^5s) on logarithmic scales for the alloy specimens FA and TSA. The ω precipitates appeared in TEM images as spheroids with an aspect ratio of about 2, elongated in the $<111>_\beta$ direction of the β-Ti matrix, throughout the ageing process. The spheroid was reduced to an equivalent-volume sphere. It is noted in Figure 11 that the average diameter of the precipitates in the FA specimen follows initially a parabolic growth law and then increase gradually, whereas when aged under tension the precipitate size increases

initially linearly with t and then increases gradually. That is, the growth of ω precipitates is governed by diffusion of Mo from the interface to the Ti matrix [26] at the initial stage of free ageing, but is interface-controlled under tensile stress. This result supports our idea that external stress influences the interface velocity, equation (5).

Fratzl et al. [26] have examined the growth of ω precipitates in a Ti-14Mo alloy aged at temperatures between 350 and 500°C by small-angle X-ray scattering, found that the precipitate size increases, in a first stage, with ageing time t as $t^{1/3}$ and interpreted as a coarsening process. This result is in disagreement with our result that the average diameter for the FA specimen first increases parabolically with t. The cause for the disagreement between our and their results is not clear. However, we would like to emphasize here that the first stage of ageing in this work corresponds evidently to a growth stage of ω precipitates before the beginning of a coarsening stage, since the hardness and the volume fraction of precipitates steeply increase in the initial stage of ageing and then continue to slowly increase up to 168 h.

To quantitatively substantiate equation (5), a further investigation of the dependence of the growth velocity of ω precipitates on the magnitude of external stress and ageing temperature will be required. The investigation is now in progress.

5. Conclusions

1. A HRTEM observation of transition phases in a Cu-1.2wt%Be-0.1wt%Co alloy aged at 320°C has revealed that the phases follow a γ" → γ" + γ' → γ sequence. The heterogeneous precipitation of the γ' phase takes place on the γ" phase.

2. The effects of an external stress on the nucleation and growth of disc-shaped γ" and plate-shaped γ' precipitates have been examined for the alloy aged at 320°C.

Application of a compressive stress along the [001] direction during ageing promotes particularly the nucleation and growth of the disc-shaped γ" variant parallel to the (001) plane amongst crystallographically-equivalent three ones and the specific four γ' variants nucleated on the γ" variant parallel to (001). However, a tensile stress does not significantly have an effect on those of γ" and γ' precipitates.

3. The acceleration of the nucleation and growth of the specific γ" and γ' variants can be well understood through the interaction energy between the stress acting on the γ" and γ' variants and the misfit strains of them.

4. The critical diameter of the disc-shaped γ" nucleus is estimated as about 1nm from evaluation of the interaction energy.

5. It is suggested that external stress does not influence the rate of diffusion but the velocity of an interface between a precipitate and a matrix.

Acknowledgements

A part of this work was conducted in the Kyoto-Advanced Nanotechnology Network, supported by the "Nanotechnology Network" of the Ministry of Education, Culture, Sports, Science and Technology (MEXT), Japan. We also thank Professor Sukedai, Okayama University of Science, for provision of the Ti-Mo alloy.

References

[1] Y. Nakada, W.C. Leslie and T.P. Churay, Trans. ASM 60 (1967) p.223.

[2] W.F. Hosford and S.P. Agrawal, Metall. Trans. 6A (1975) p.487.

[3] T. Mori and M. Horie, J. Jpn. Inst. Metall. 39 (1975) p.581.

[4] G. Sauthoff, Z. Metallkde. 68 (1977) p.500.

[5] T. Eto, A. Sato and Mori T, Acta Metall. 26 (1978) p.499.

[6] Y. Tanaka, A. Sato and T. Mori, Acta Metall. 26 (1978) p.529.

[7] B. Skrotzki, G.J. Shiflet and E.A. Starke Jr, Metall. Mater. Trans. 27A (1996) p.3431.

[8] H. Nishizawa, E. Sukedai, W. Liu and H. Hashimoto, Mater. Trans. JIM 39 (1998) p.609.

[9] A.W. Zhu and E.A. Starke Jr, Acta Mater. 49 (2001) p.2285.

[10] R. Monzen, C. Watanabe, T. Seo and T.Sakai, Philos. Mag. Lett. 85 (2005) p.603.

[11] R. Monzen, T. Terazawa and C. Watanabe, Mater. Sci. Forum (2010) p.654 p.922.

[12] R. Monzen, C. Watanabe, T. Seo and T. Sakai, Mater. Trans. 12 (2006) p.2925.

[13] R.J. Rioja and D.E. Laughlin, Acta Metall. 28 (1980) p.1301.

[14] C. Watanabe, T. Sakai and R. Monzen, Phil. Mag. A 9 (2008) p.1401.

[15] D.B. Williams and E.P. Butler, Int. Met. Rev. 26 (1981) p.153.

[16] A. Yamamoto, R. Nozato, T. Morimoto and H. Tsubakino, Mater. Trans. 34 (1993) p.312.

[17] H. Tanimura, G. Wassermann and Z. Metallkde. 25 (1933) p.179.

[18] L. Yagmur, O. Duygulu and B. Aydemir, Mater. Sci. Eng. A 523 (2011) p.4147.

[19] J.D. Eshelby, Proc. R. Soc. A 241 (1957) p.376.

[20] M. Volmer and A.Weber, Z. Phys. Chem. 119 (1926) p.277.

[21] T. Eto, M. Nachi and T. Mori, Trans. JIM 20 (1979) p.459.

[22] J.W. Christian, *The Theory of Transformation in Metals and Alloys*, 3rd ed., Vol. 1, Pergamon Press, Oxford, 2002, p.480.

[23] H.I. Aaronson, M. Enomoto and J.K. Lee, *Mechanisms of Diffusional Phase Transformations in Metals and Alloys*, CRC Press, New York, 2010.

[24] G. Chen, G. Spanos, R.A. Matsumura and W.T. Reynolds Jr, Acta Mater. 53 (2005) p.895.

[25] C. Watanabe and R. Monzen, Solid State Phenomena 172-174 (2011) p.432.

[26] P. Fratzl, F. Langmayr, G. Vogl and W. Miekeley, Acta Meter. Mater. 39 (1991) p.753.

Table 1. Misfit strains of the GP zone [10] and γ", γ' and γ phases [14] in Cu-Be single-crystal specimens, obtained by length-change measurements.

	GP zone	γ"	γ'	γ
$\varepsilon_{11}\ (=\varepsilon_{22})$	–0.01	–0.01	–0.03	–0.03
ε_{33}	–0.10	–0.11	–0.09	–0.08

Table 2. Notation of the three γ" and twelve γ' variants.

Variant notation	γ" variant	Variant notation	γ' variant	
I	$(001)_\alpha$ // $(001)_{\gamma''}$ $[110]_\alpha$ // $[100]_{\gamma''}$	I	-1 $(1\bar{1}\bar{2})_\alpha$ // $(0\bar{1}\bar{2})_{\gamma'}$	$[110]_\alpha$ // $[100]_{\gamma'}$
			-2 $(1\bar{1}3)_\alpha$ // $(0\bar{1}3)_{\gamma'}$	
			-3 $(112)_\alpha$ // $(102)_{\gamma'}$	$[1\bar{1}0]_\alpha$ // $[0\bar{1}0]_{\gamma'}$
			-4 $(11\bar{3})_\alpha$ // $(10\bar{3})_{\gamma'}$	
II	$(010)_\alpha$ // $(010)_{\gamma''}$ $[101]_\alpha$ // $[001]_{\gamma''}$	II	-1 $(\bar{1}21)_\alpha$ // $(120)_{\gamma'}$	$[101]_\alpha$ // $[001]_{\gamma'}$
			-2 $(13\bar{1})_\alpha$ // $(1\bar{3}0)_{\gamma'}$	
			-3 $(121)_\alpha$ // $(0\bar{2}\bar{1})_{\gamma'}$	$[10\bar{1}]_\alpha$ // $[\bar{1}00]_{\gamma'}$
			-4 $(\bar{1}3\bar{1})_\alpha$ // $(03\bar{1})_{\gamma'}$	
III	$(100)_\alpha$ // $(100)_{\gamma''}$ $[011]_\alpha$ // $[010]_{\gamma''}$	III	-1 $(2\bar{1}1)_\alpha$ // $(201)_{\gamma'}$	$[011]_\alpha$ // $[010]_{\gamma'}$
			-2 $(31\bar{1})_\alpha$ // $(\bar{3}01)_{\gamma'}$	
			-3 $(211)_\alpha$ // $(2\bar{1}0)_{\gamma'}$	$[01\bar{1}]_\alpha$ // $[00\bar{1}]_{\gamma'}$
			-4 $(3\bar{1}\bar{1})_\alpha$ // $(\bar{3}\bar{1}0)_{\gamma'}$	

Table 3. Number density of γ" variants in Cu-Be-Co specimens, free-aged (FA), compressive-stress-aged (CSA) and tensile-stress-aged (TSA) at 320°C for 3h.

Variant notation	Density(10^{23} m^{-3})		
	FA	CSA	TSA
I	1.5 ± 0.2	2.5 ± 0.2	1.1 ± 0.1
II		1.5 ± 0.2	1.6 ± 0.2
III			

Table 4. Diameter of disc-shaped γ" variants in Cu-Be-Co specimens, aged at 320°C for 2h and then FA, CSA or TSA at 320°C for 1h.

Variant notation	Size (nm)		
	FA	CSA	TSA
I	10 ± 1.2	13 ± 1.4	10 ± 1.2
II		10 ± 1.3	10 ± 1.1
III			

Table 5. Fraction of the number $N_{3\gamma''+\gamma'}$ of γ" precipitates consisting of three Be-layers with γ' phase to the total number $N_{3\gamma''}$ of γ" precipitates consisting of three Be-layers for the specimen, aged at 320°C for 3h and then CSA at 320°C for 1h, and that of the number $N_{6\gamma''+\gamma'}$ of γ" precipitates consisting of six Be-layers with γ' phase to the total number $N_{6\gamma''}$ of γ" precipitates consisting of six Be-layers for the specimen, aged at 320°C for 5h and then FA or TSA at 320°C for 1h.

Variant notation	$N_{3\gamma''+\gamma'}/N_{3\gamma''}$	$N_{6\gamma''+\gamma'}/N_{6\gamma''}$	
	CSA	FA	TSA
I-1 – I-4	93%	87%	80%
II-1 – II-4 III-1 – III-4	35%	85%	85%

Table 6. Length of plate-shaped γ' variants in the specimens, aged at 320°C for 3h, compressive-stress-aged at 320°C for 1h and then FA, CSA or TSA at 320°C for 2h.

Variant notation	Size (nm)		
	FA	CSA	TSA
I-1 – I-4	57 ± 13	72 ± 14	56 ± 14
II-1 – II-4 III-1 – III-4	50 ± 11	56 ± 13	50 ± 11

Figure Captions

Figure 1. Age hardening curves of Cu-1.2Be-0.1Co specimens, free-aged (FA), compressive-stress-aged (CSA) and tensile-stress-aged (TSA) at 320°C.

Figure 2. HRTEM image of γ" precipitates in a Cu-Be-Co specimen aged at 320°C for 2h. The zone axis is along $[110]_{\alpha}$.

Figure 3. HRTEM image of a precipitate consisting of γ" and γ' phases in a Cu-Be-Co specimen aged at 320°C for 6h. The zone axis is along $[110]_{\alpha}$.

Figure 4. HRTEM images of a precipitate consisting of γ" and γ' phases in a Cu-Be-Co specimen aged at 320°C for 6h. (b) Enlarged inverse fast Fourier transformation (IFFT) image of the outlined region in (a). (c) Schematic illustration of the IFFT image showing a γ"/Cu lattice-spacing ratio closer to 5 : 4 at the γ"/Cu interface. The zone axis is parallel to $[110]_{\alpha}$.

Figure 5. TEM images and SADPs of (a) FA, (b) CSA and (c) TSA specimens. Ageing was carried out at 320°C for 3h. The arrows in (b) and (c) indicate the applied stress axis. The zone axis is parallel to $[100]_{\alpha}$.

Figure 6. Effect of free, compressive-stress and tensile-stress ageing at 320°C on the number density of disc-shaped γ" precipitates.

Figure 7. TEM image of γ" precipitates in a Cu-Be-Co specimen, FA at 320°C for 2h and then CSA at 320°C for 1h. The zone axis is parallel to $[100]_{\alpha}$. The arrow indicates the stress axis.

Figure 8. HRTEM image of a precipitate consisting of γ" and γ' phases in a Cu-Be-Co specimen, FA at 320°C for 3h and then CSA at 320°C for 1h. The zone axis is parallel to $[110]_{\alpha}$. The arrow indicates the stress axis.

Figure 9. TEM image of γ' variants I-1 and I-2 in a specimen, aged at 320°C for 3h and then CSA at 320°C for 3h. The zone axis is parallel to $[110]_{\alpha}$. The arrow indicates the stress axis.

Figure 10. Natural logarithm of relative nucleation rates of γ" precipitates plotted against $\cos^2\theta$.

Figure 11. Variation in the average diameters of ω precipitates with ageing time *t* for a Ti-20Mo alloy aged at 350°C under no stress and a tensile stress of 400MPa.

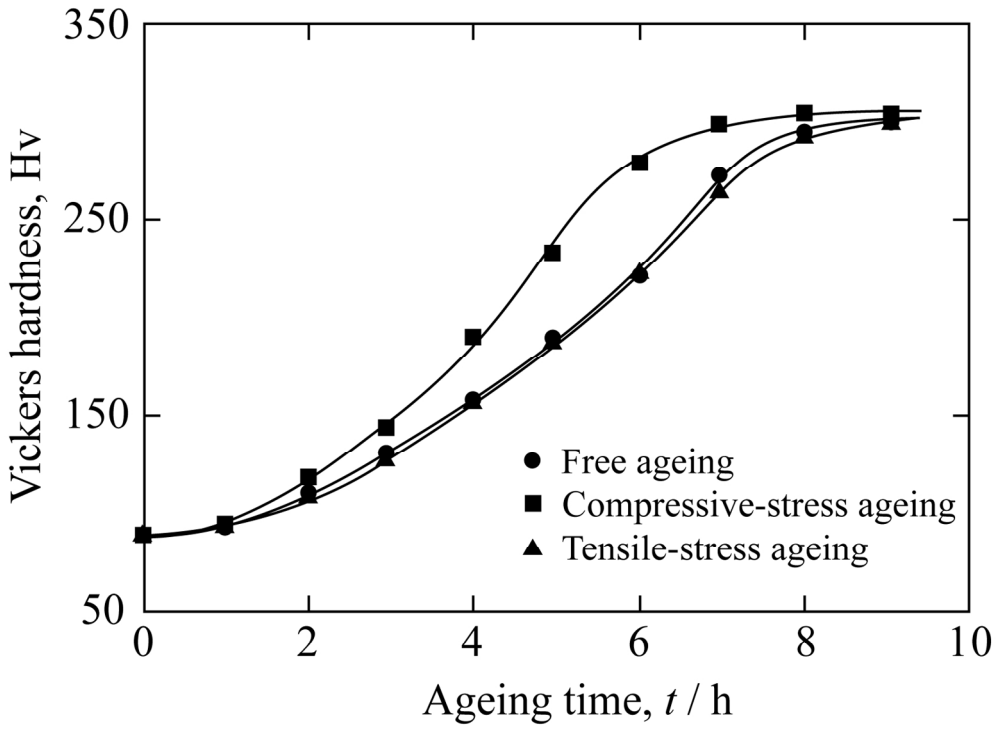

Figure 1. Age hardening curves of Cu-1.2Be-0.1Co specimens, free-aged (FA), compressive-stress-aged (CSA) and tensile-stress-aged (TSA) at 320°C.
143x109mm (300 x 300 DPI)

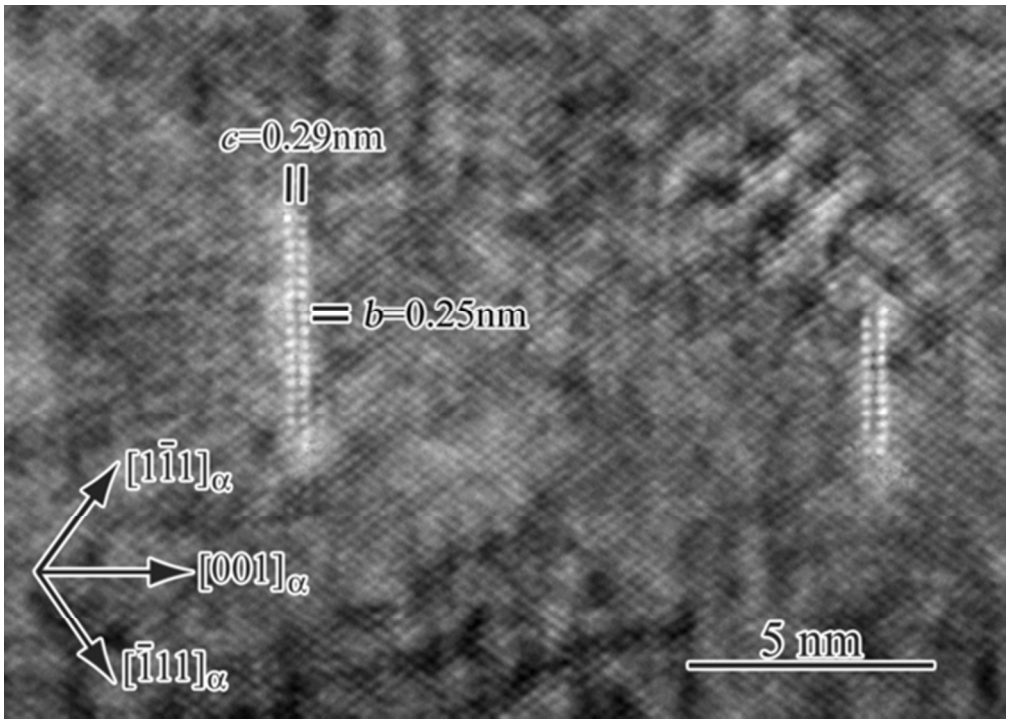

Figure 2. HRTEM image of γ" precipitates in a Cu-Be-Co specimen aged at 320°C for 2h. The zone axis is along $[110]_\alpha$.
49x35mm (300 x 300 DPI)

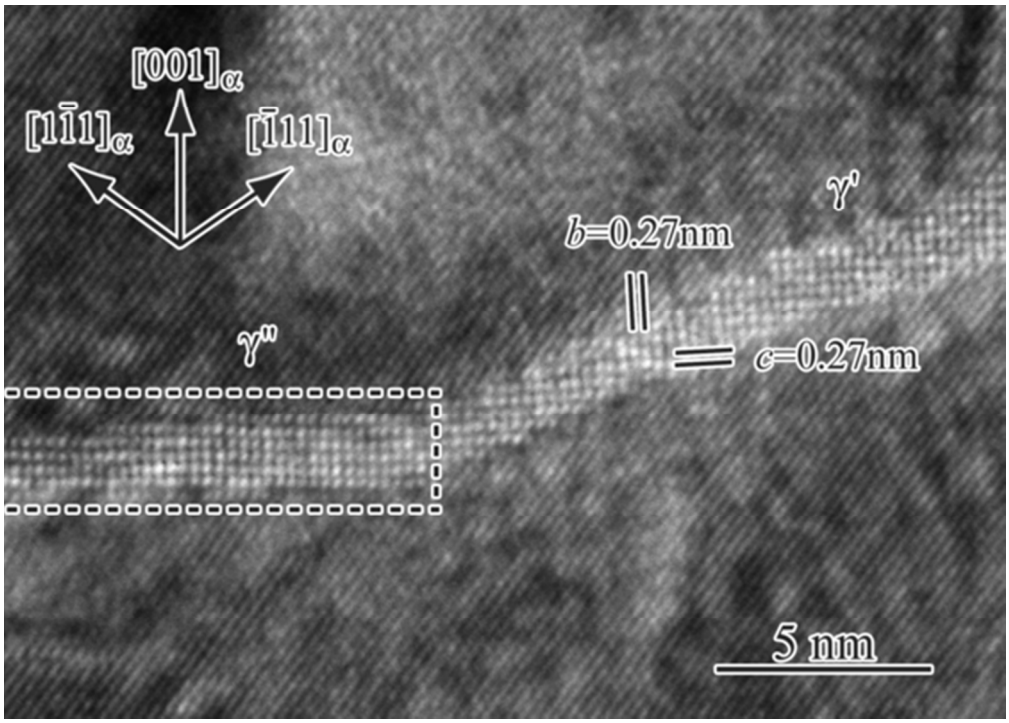

Figure 3. HRTEM image of a precipitate consisting of γ" and γ' phases in a Cu-Be-Co specimen aged at 320°C for 6h. The zone axis is along $[110]_{\alpha}$.
49x35mm (300 x 300 DPI)

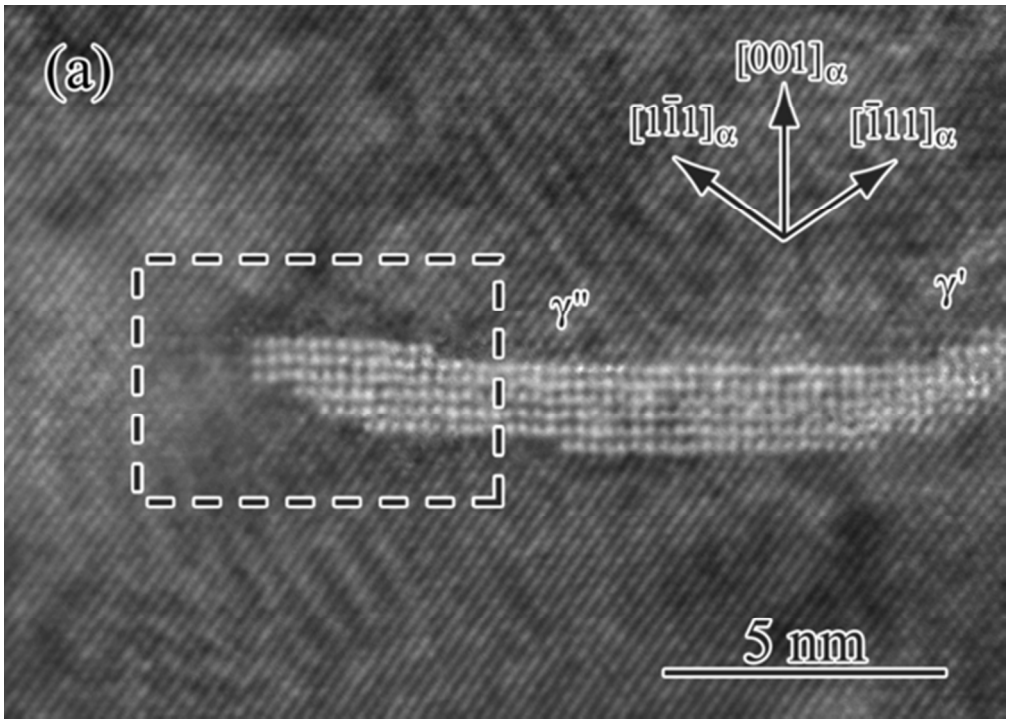

Figure 4. HRTEM images of a precipitate consisting of γ" and γ' phases in a Cu-Be-Co specimen aged at 320°C for 6h. (b) Enlarged inverse fast Fourier transformation (IFFT) image of the outlined region in (a). (c) Schematic illustration of the IFFT image showing a γ"/Cu lattice-spacing ratio closer to 5 : 4 at the γ"/Cu interface. The zone axis is parallel to $[110]_{\alpha}$.
49x35mm (300 x 300 DPI)

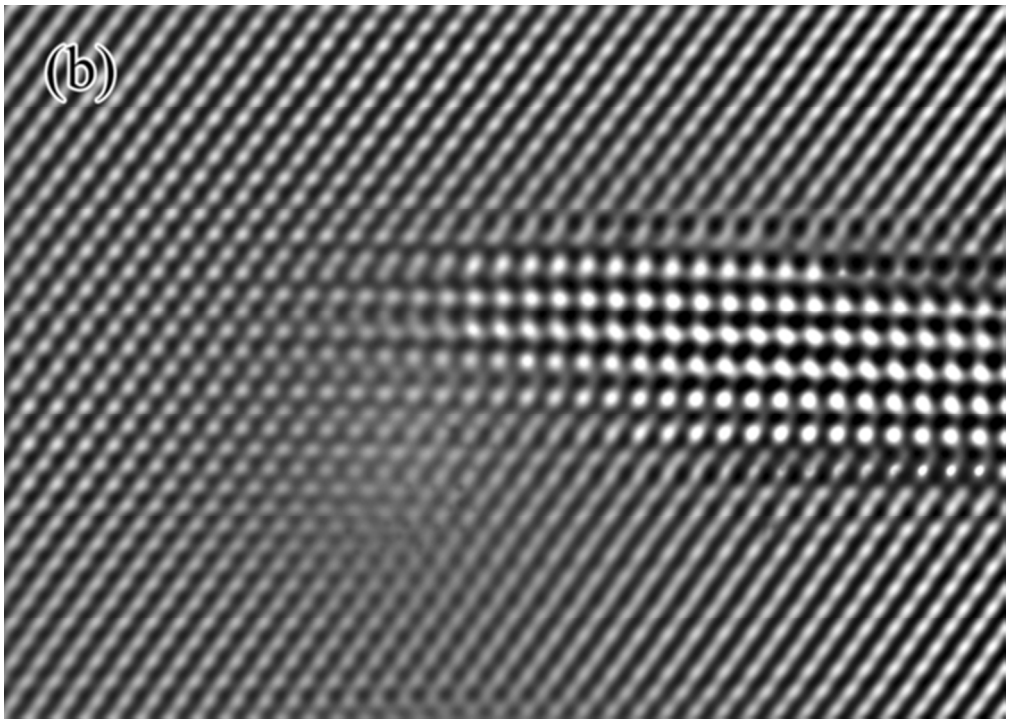

Figure 4. HRTEM images of a precipitate consisting of γ″ and γ′ phases in a Cu-Be-Co specimen aged at 320°C for 6h. (b) Enlarged inverse fast Fourier transformation (IFFT) image of the outlined region in (a). (c) Schematic illustration of the IFFT image showing a γ″/Cu lattice-spacing ratio closer to 5 : 4 at the γ″/Cu interface. The zone axis is parallel to $[110]_{\alpha}$.
49x35mm (300 x 300 DPI)

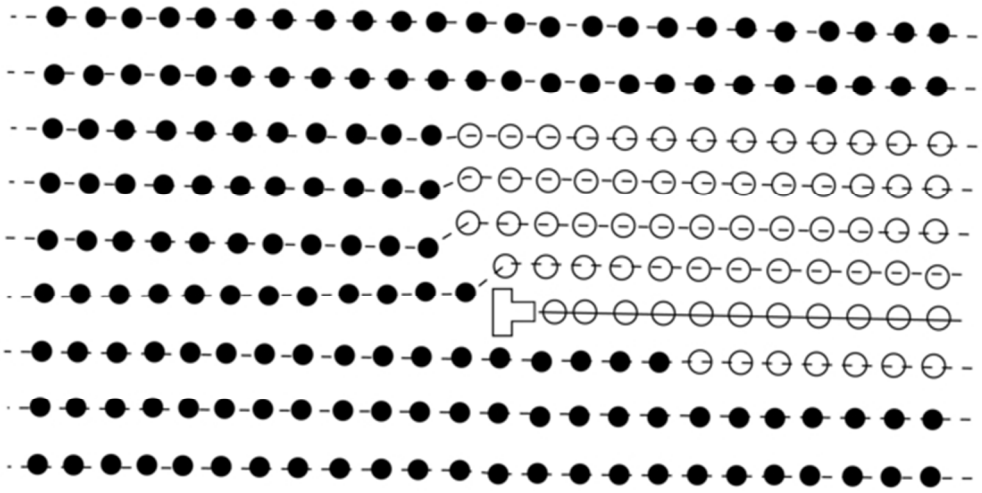

Figure 4. HRTEM images of a precipitate consisting of γ″ and γ′ phases in a Cu-Be-Co specimen aged at 320°C for 6h. (b) Enlarged inverse fast Fourier transformation (IFFT) image of the outlined region in (a). (c) Schematic illustration of the IFFT image showing a γ″/Cu lattice-spacing ratio closer to 5 : 4 at the γ″/Cu interface. The zone axis is parallel to $[110]_{\alpha}$.
54x27mm (300 x 300 DPI)

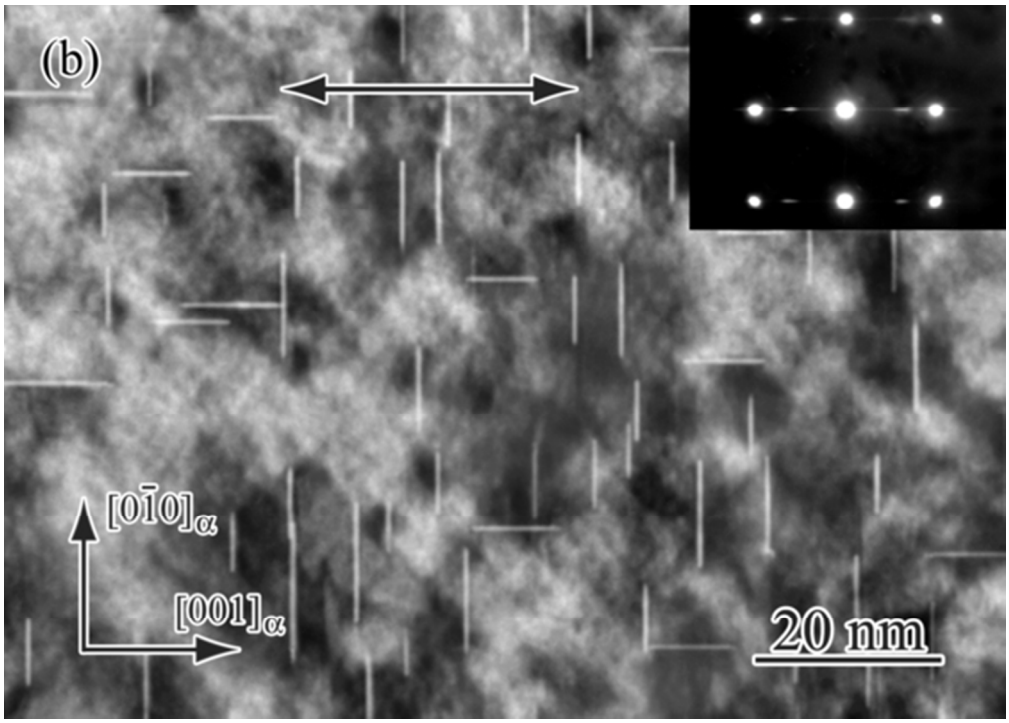

Figure 5. TEM images and SADPs of (a) FA, (b) CSA and (c) TSA specimens. Ageing was carried out at 320°C for 3h. The arrows in (b) and (c) indicate the applied stress axis. The zone axis is parallel to $[100]_\alpha$.
49x35mm (300 x 300 DPI)

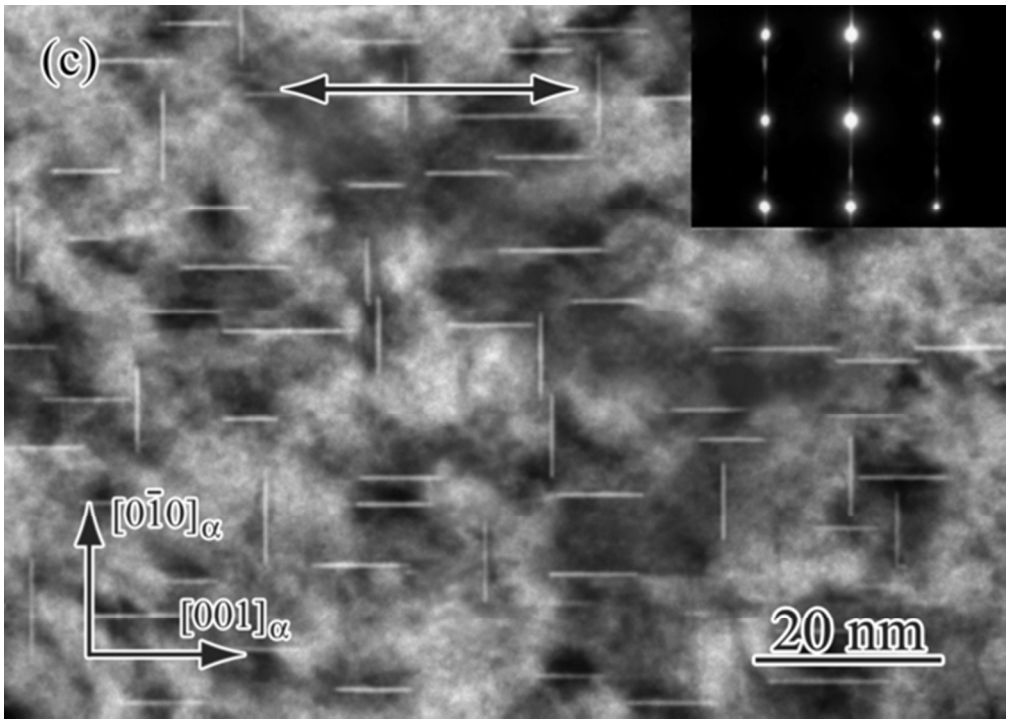

Figure 5. TEM images and SADPs of (a) FA, (b) CSA and (c) TSA specimens. Ageing was carried out at 320°C for 3h. The arrows in (b) and (c) indicate the applied stress axis. The zone axis is parallel to $[100]_\alpha$.
49x35mm (300 x 300 DPI)

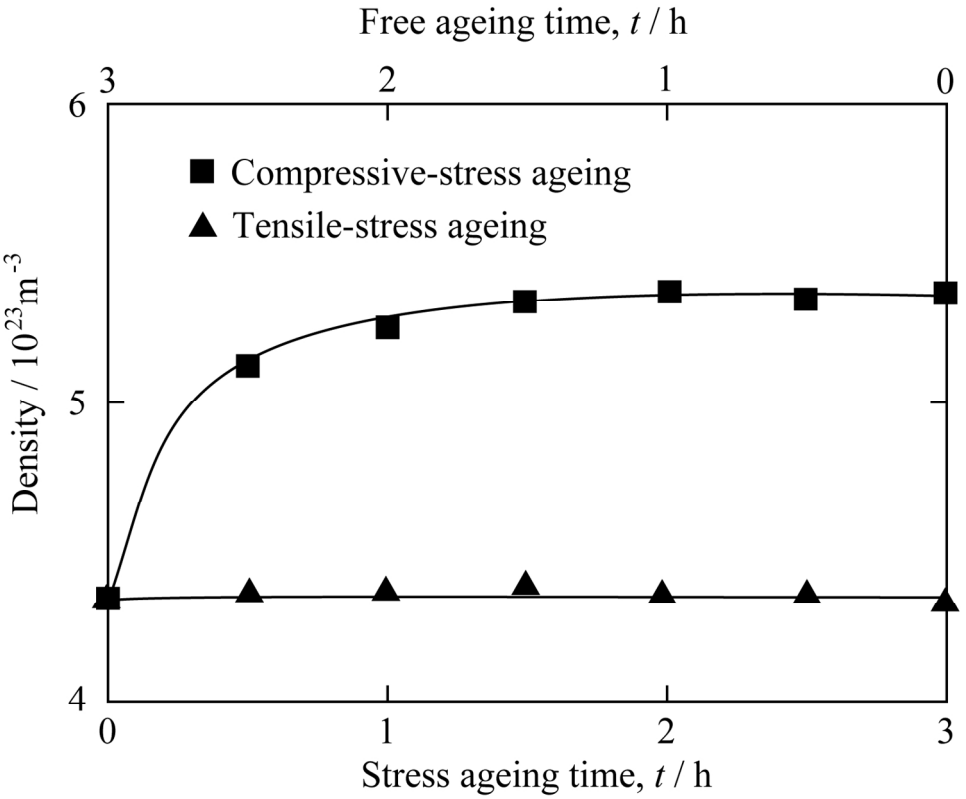

Figure 6. Effect of free, compressive-stress and tensile-stress ageing at 320°C on the number density of disc-shaped γ" precipitates.
141x114mm (300 x 300 DPI)

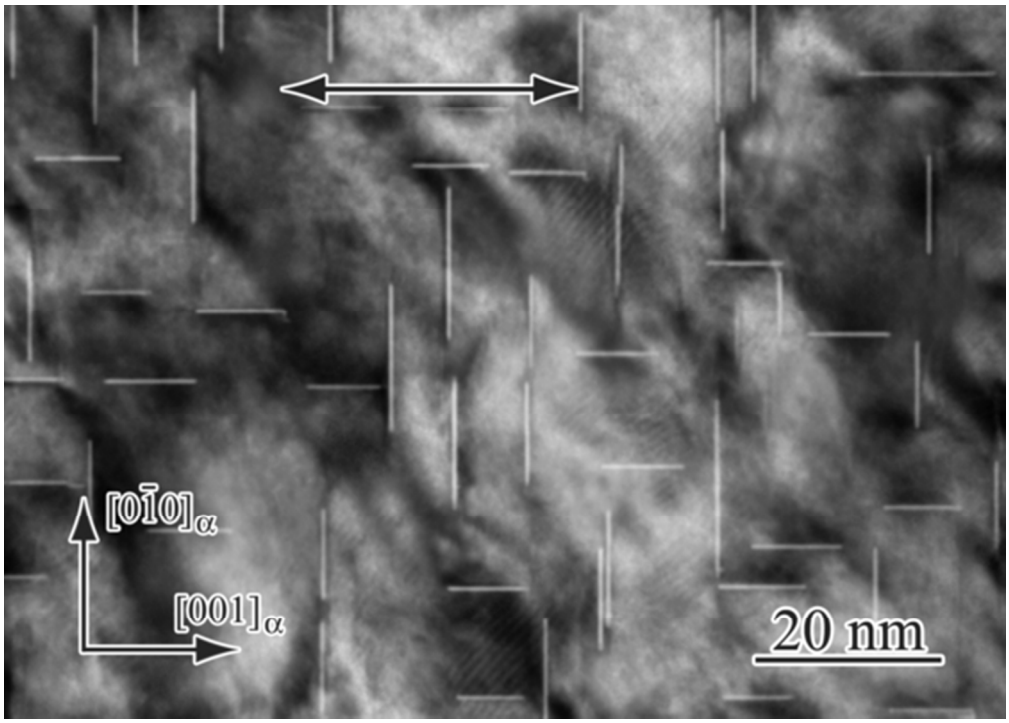

Figure 7. TEM image of γ" precipitates in a Cu-Be-Co specimen, FA at 320°C for 2h and then CSA at 320°C for 1h. The zone axis is parallel to $[100]_\alpha$. The arrow indicates the stress axis.
49x35mm (300 x 300 DPI)

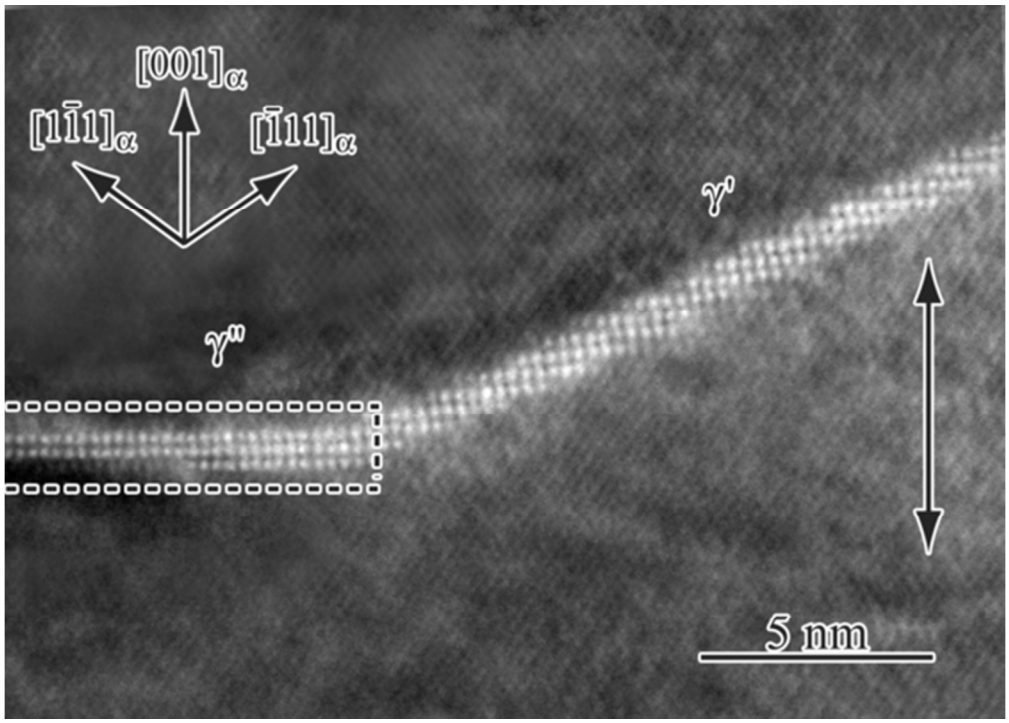

Figure 8. HRTEM image of a precipitate consisting of γ'' and γ' phases in a Cu-Be-Co specimen, FA at 320°C for 3h and then CSA at 320°C for 1h. The zone axis is parallel to $[110]_{\alpha}$. The arrow indicates the stress axis.
49x35mm (300 x 300 DPI)

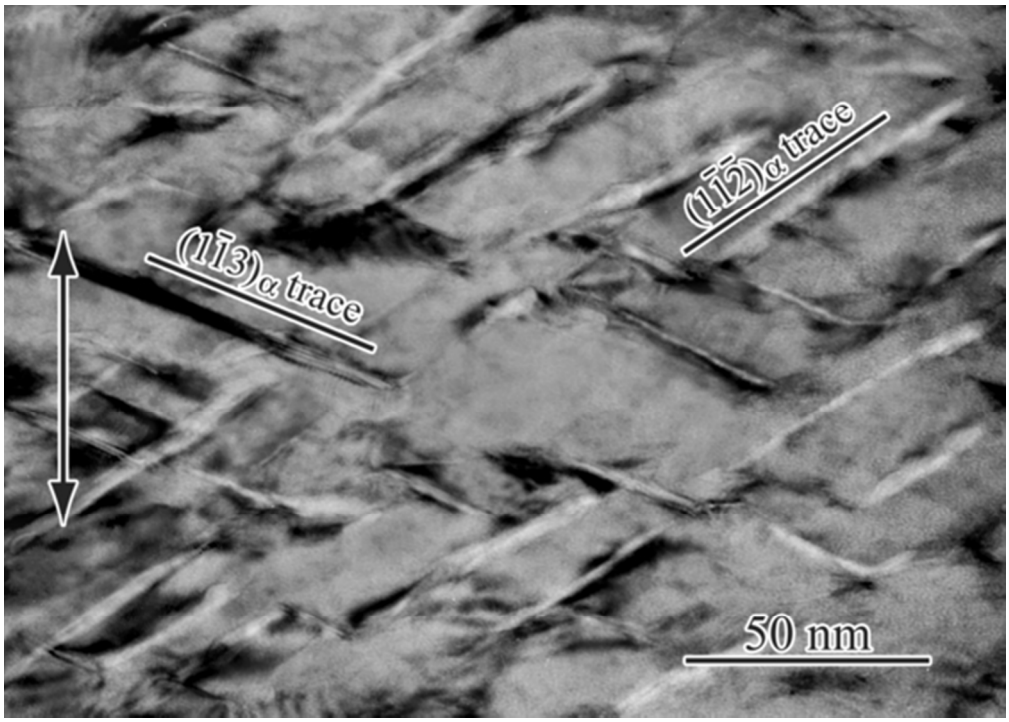

Figure 9. TEM image of γ′ variants I-1 and I-2 in a specimen, aged at 320°C for 3h and then CSA at 320°C for 3h. The zone axis is parallel to $[110]_\alpha$. The arrow indicates the stress axis.
49x35mm (300 x 300 DPI)

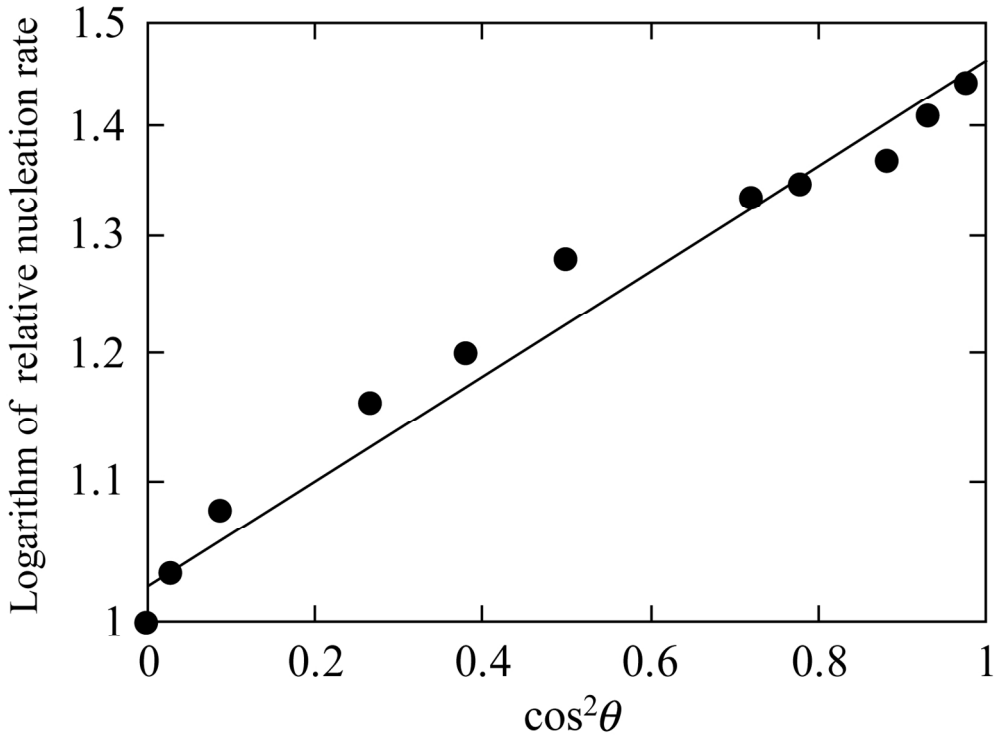

Figure 10. Logarithm of relative nucleation rates of γ″ precipitates plotted against cos2θ.
141x106mm (300 x 300 DPI)

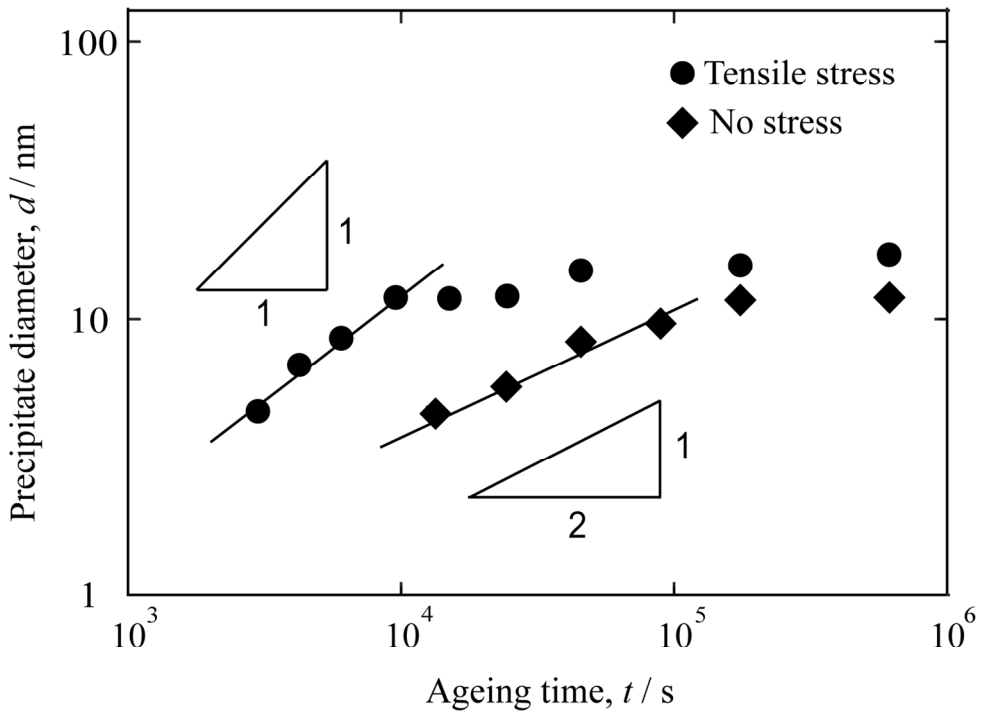

Figure 11. Variation in the average diameters of ω precipitates with ageing time *t* for a Ti-20Mo alloy aged at 350°C under no stress and a tensile stress of 400MPa.
137x103mm (300 x 300 DPI)